

Article

# Surface Waves Propagating on Grounded Anisotropic Dielectric Slab

Zhuozhu Chen <sup>1,\*</sup> and Zhongxiang Shen <sup>2</sup>

<sup>1</sup> School of Information Engineering, Guangdong University of Technology, Guangzhou 510006, China

<sup>2</sup> School of Electrical and Electronic Engineering, Nanyang Technological University, Singapore 639798, Singapore; ezxshen@ntu.edu.sg

\* Correspondence: chen0855@e.ntu.edu.sg; Tel.: +65-6516-1044

Received: 27 November 2017; Accepted: 9 January 2018; Published: 11 January 2018

**Abstract:** This paper investigates the characteristics of surface waves propagating on a grounded anisotropic dielectric slab. Distinct from the existing analyses that generally assume that the fields of surface wave uniformly distribute along the transverse direction of the infinitely large grounded slab, our method takes into account the field variations along the transverse direction of a finite-width slab. By solving Maxwell's equations in closed-form, it is revealed that no pure transverse magnetic (TM) or transverse electric (TE) mode exists if the fields are non-uniformly distributed along the transverse direction of the grounded slab. Instead, two hybrid modes, namely quasi-TM and quasi-TE modes, are supported. In addition, the propagation characteristics of two hybrid modes supported by the grounded anisotropic slab are analyzed in terms of the slab thickness, slab width, as well as the relative permittivity tensor of the anisotropic slab. Furthermore, different methods are employed to compare the analyses, as well as to validate our derivations. The proposed method is very suitable for practical engineering applications.

**Keywords:** anisotropic metamaterial; grounded dielectric slab; guided waves; surface waves

## 1. Introduction

Over recent decades, surface waves have attracted extensive attention due to their unique characteristics of existing at the interface of two different media with the field exponentially decaying away from the interface. For example, Dyakonov surface waves have been investigated thoroughly in several literatures [1–3]. The characteristics of the surface waves propagating at the interfaces between isotropic-to-isotropic, isotropic-to-anisotropic, and isotropic-to-indefinite media have been rigorously studied in [4–8]. Moreover, surface waves have also been found in many structures, such as dielectric rod [9], uniaxial and biaxial slab waveguides [10,11], plasma slab [12], chiral material [13], and photonic crystal [14], to name only a few.

Among all of the geometries of supporting surface waves, one of the best-known structures is the grounded dielectric slab. It is known that the infinitely large grounded dielectric slab can support pure transverse magnetic (TM) and transverse electric (TE) surface wave modes, and their propagating constants on isotropic slab were analyzed in [4], the corresponding fields and power of the surface waves were studied in [15]. In addition to the case of isotropic grounded slab, the guidance conditions of TM and TE surface waves in grounded anisotropic slab were considered in [16]. The solution of suppressing surface waves on grounded anisotropic slab was explored in [17]. Furthermore, investigations were also focused on the radiation conditions of surface wave on grounded dielectric slabs, which have been employed for designing wideband, low-profile, as well as high gain antennas [18–20].

Although a lot of studies have been carried out to characterize surface waves propagating along a grounded dielectric slab, the analyses only focus on structures that are of infinite length and width, and assume that there is no field variation along the direction orthogonal to the propagation direction

of surface waves. To the best of our knowledge, no detailed analysis has been introduced for the case that the fields are non-uniformly distributed along the direction transverse to the propagation direction, which is a more practical concern for most engineers. In addition, most substrates used in real applications exhibit nonnegligible anisotropic properties due to either the intrinsic anisotropy of the material or the manufacturing process [21]. The effect of the anisotropy of the material on the propagation characteristics of surface waves is another concern for practical engineering.

This paper investigates the characteristics of surface waves propagating on a grounded anisotropic dielectric slab, especially focuses on the slab with finite width. By assuming that the surface waves are propagating along the longitudinal direction of the slab, the field variations along the transverse direction are considered. Different methods are compared to analyze the propagation characteristics, as well as to validate our derivations. The main contributions of our work are as follows. (i) It is revealed that no pure TM or TE mode exists on the grounded infinitely large slab if the field is non-uniformly distributed along the direction orthogonal to the propagation direction; (ii) Closed-form analytical expressions are derived to theoretically study the characteristics of quasi-TM and quasi-TE surface modes on the finite-width grounded anisotropic grounded slab. It is found that surface waves propagate away from the longitudinal direction of the finite-width slab with some certain angle, and the angle decreases as the slab width increases; (iii) Different from the existing analyses of surface waves whose fields distribute uniformly along the transverse direction of the infinitely large slab, our method takes into account the variations of the fields distributed on the transverse direction of the grounded anisotropic slab, which has a more practical relevance and can provide a more accurate solution for engineering applications such as designing wideband and high gain antennas based on grounded dielectric slabs [9,18–20]. It is worth mentioning that our method is also suitable for grounded isotropic dielectric slab.

## 2. Characteristics of Surface Waves Propagating on Grounded Anisotropic Slab

### 2.1. Infinitely Large Anisotropic Grounded Slab

Figure 1 shows the geometry of the anisotropic slab backed by a perfect electric conductor. We assume that the grounded slab is infinite in both  $x$  and  $y$  directions, the surface waves propagate along the longitudinal  $+x$  direction with an  $e^{-j\beta_x x}$  propagation factor. The thickness of the slab is  $t$ . The slab is considered as anisotropic as a general discussion, and the relative permittivity  $\bar{\epsilon}$  and permeability  $\bar{\mu}$  of the anisotropic slab are expressed as:

$$\bar{\epsilon} = \begin{bmatrix} \epsilon_x & 0 & 0 \\ 0 & \epsilon_y & 0 \\ 0 & 0 & \epsilon_z \end{bmatrix}, \bar{\mu} = \begin{bmatrix} \mu_x & 0 & 0 \\ 0 & \mu_y & 0 \\ 0 & 0 & \mu_z \end{bmatrix}, \quad (1)$$

where the diagonal elements represent the eigenvalues of  $\bar{\epsilon}$  and  $\bar{\mu}$ , respectively, and their directions constitute the principle axes of the anisotropic slab. In order to analyze the characteristics of surface waves propagating along the grounded anisotropic dielectric slab, we separately consider the fields in anisotropic and air regions, then solve Maxwell's equations and apply boundary conditions across the interface. For the considered structure, the E-field and H-field along the  $x$  direction for both regions are expressed as:

Region I

$$E_x^I = A_I f_e(y) e^{-j\beta_x x} \sin(k_z z), \quad (2)$$

$$H_x^I = B_I f_h(y) e^{-j\beta_x x} \cos(k_z z), \quad (3)$$

Region II

$$E_x^{II} = A_{II} f_e(y) e^{-j\beta_x x} e^{-k_0 z}, \quad (4)$$

$$H_x^{II} = B_{II} f_h(y) e^{-j\beta_x x} e^{-k_0 z}, \quad (5)$$

where  $A_I$ ,  $A_{II}$ ,  $B_I$ , and  $B_{II}$  are the amplitude coefficients of the corresponding fields in each region.  $\beta_x$  is the phase constant of surface waves along the  $x$  direction.  $k_z$  is the wavenumber in the anisotropic

medium in the  $z$  direction. The sine function of  $E_x^I$  and cosine function of  $H_x^I$  in the anisotropic medium are selected due to the vanishing electric field and maximum magnetic field on the perfect electric conductor (PEC) ground plane, respectively. Due to the fields of surface waves decaying exponentially away in air from the interface, the  $z$  component of fields in air region is expressed as  $e^{-k_{0z}z}$ , with  $k_{0z}$  real and positive. In addition,  $f_e(y)$  and  $f_h(y)$  represent the  $y$  components of E-field and H-field, respectively. For the infinitely large slab, we assume that the propagation constant in the  $y$  direction is  $R_y$ ,  $f_e(y)$  and  $f_h(y)$ , then satisfy the following form:

$$f_e(y) = f_h(y) = f(y) = \begin{cases} e^{-R_y y} & (y \geq 0) \\ e^{R_y y} & (y \leq 0) \end{cases} \quad (6)$$

If  $R_y = 0$ , then  $\partial f(y)/\partial y = 0$ , which indicates that the field has no variation in the  $y$  direction. On the other hand, if  $R_y \neq 0$ , the field of surface wave is non-uniformly distributed along the  $y$  direction.

By solving Maxwell's equations based on Equations (2)–(5), the E- and H-fields in both anisotropic slab and air regions in  $y$  and  $z$  directions are found as:

Region I

$$E_y^I = \frac{e^{-j\beta_x x} \sin(k_z z)}{j(\epsilon_y \mu_z k_0^2 - \beta_x^2)} [\beta_x A_I \frac{\partial f_e(y)}{\partial y} - \omega \mu_0 \mu_z k_z B_I f_h(y)], \quad (7)$$

$$H_y^I = \frac{e^{-j\beta_x x} \cos(k_z z)}{j(\epsilon_z \mu_y k_0^2 - \beta_x^2)} [\beta_x B_I \frac{\partial f_h(y)}{\partial y} - \omega \epsilon_0 \epsilon_z k_z A_I f_e(y)], \quad (8)$$

$$E_z^I = \frac{e^{-j\beta_x x} \cos(k_z z)}{j(\epsilon_z \mu_y k_0^2 - \beta_x^2)} [\beta_x k_z A_I f_e(y) - \omega \mu_0 \mu_y B_I \frac{\partial f_h(y)}{\partial y}], \quad (9)$$

$$H_z^I = \frac{e^{-j\beta_x x} \sin(k_z z)}{j(\epsilon_y \mu_z k_0^2 - \beta_x^2)} [-\beta_x k_z B_I f_h(y) + \omega \epsilon_0 \epsilon_y A_I \frac{\partial f_e(y)}{\partial y}]. \quad (10)$$

Region II

$$E_y^{II} = \frac{e^{-j\beta_x x} e^{-k_{0z} z}}{j(k_0^2 - \beta_x^2)} [\beta_x A_{II} \frac{\partial f_e(y)}{\partial y} - \omega \mu_0 k_{0z} B_{II} f_h(y)], \quad (11)$$

$$H_y^{II} = \frac{e^{-j\beta_x x} e^{-k_{0z} z}}{j(k_0^2 - \beta_x^2)} [\beta_x B_{II} \frac{\partial f_h(y)}{\partial y} + \omega \epsilon_0 k_{0z} A_{II} f_e(y)], \quad (12)$$

$$E_z^{II} = \frac{e^{-j\beta_x x} e^{-k_{0z} z}}{j(k_0^2 - \beta_x^2)} [-\beta_x k_{0z} A_{II} f_e(y) - \omega \mu_0 B_{II} \frac{\partial f_h(y)}{\partial y}], \quad (13)$$

$$H_z^{II} = \frac{e^{-j\beta_x x} e^{-k_{0z} z}}{j(k_0^2 - \beta_x^2)} [-\beta_x k_{0z} B_{II} f_h(y) + \omega \epsilon_0 A_{II} \frac{\partial f_e(y)}{\partial y}]. \quad (14)$$

Based on the field distributions and boundary conditions, the characteristics of the surface waves can be analyzed, as follows.

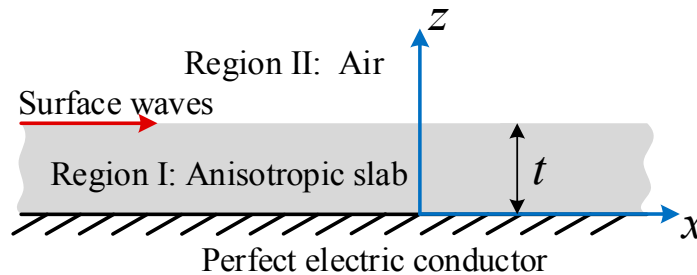


**Figure 1.** Surface waves on the interface of air region and grounded anisotropic slab with infinite length in  $x$  and  $y$  directions.

### 2.1.1. TM Mode Surface Wave

For the pure TM surface wave, it is known that  $B_I = B_{II} = 0$ , the continuity conditions of  $E_x$  and  $E_y$  at the interface  $z = t$  give

$$A_I \sin(k_z t) = A_{II} e^{-k_{0z} t}, \tag{15}$$

$$\frac{\partial f(y)}{\partial y} \frac{A_I \sin(k_z t)}{\epsilon_y \mu_z k_0^2 - \beta_x^2} = \frac{\partial f(y)}{\partial y} \frac{A_{II} e^{-k_{0z} t}}{k_0^2 - \beta_x^2}, \tag{16}$$

which lead to

$$\epsilon_y \mu_z = 1, \tag{17}$$

or

$$\frac{\partial f(y)}{\partial y} = 0. \tag{18}$$

It is obvious that Equation (17) is not satisfied since the dielectric slab cannot be air for our discussion. Therefore, Equation (18) is the only solution, indicating that for pure TM surface wave propagating along the  $x$  direction of the grounded anisotropic slab, the field distribution along the  $y$  direction must be uniform.

### 2.1.2. TE Mode Surface Wave

For the pure TE surface wave, it is obvious that  $A_I = A_{II} = 0$ . Similarly, according to the boundary conditions of  $H_x$  and  $H_y$  at the interface  $z = t$ , Equation (18) is also satisfied.

### 2.1.3. Hybrid Mode Surface Wave

Based on the above discussions, it is concluded that if the pure TM or TE surface wave exists on the grounded dielectric slab, the field distribution along the  $y$  direction must be uniform. In other words, if  $\partial f(y)/\partial y \neq 0$  or  $R_y \neq 0$ , hybrid mode surface waves that consist of quasi-TM mode with small  $H_x$  and quasi-TE mode with small  $E_x$  propagate along the slab. In this case, the continuity of tangential fields across the interface  $z = t$  leads to:

$$\begin{aligned} &\beta_x^2 R_y^2 k_0^2 (1 - \epsilon_z \mu_y) (1 - \epsilon_y \mu_z) \\ &= [\epsilon_z k_z (k_0^2 - \beta_x^2) + k_{0z} (\epsilon_z \mu_y k_0^2 - \beta_x^2) \tan(k_z t)] [\mu_z k_z (k_0^2 - \beta_x^2) \\ &\quad - k_{0z} (\epsilon_y \mu_z k_0^2 - \beta_x^2) \cot(k_z t)]. \end{aligned} \tag{19}$$

By applying Maxwell's equation, the dispersion relations in both regions are:

Region I

$$\begin{aligned} &\beta_x^2 R_y^2 k_z^2 \left( \frac{1}{\epsilon_z \mu_y k_0^2 - \beta_x^2} - \frac{1}{\epsilon_y \mu_z k_0^2 - \beta_x^2} \right)^2 = -k_0^2 \left( \epsilon_x + \frac{\epsilon_y R_y^2}{\epsilon_y \mu_z k_0^2 - \beta_x^2} - \frac{\epsilon_z k_z^2}{\epsilon_z \mu_y k_0^2 - \beta_x^2} \right) (\mu_x \\ &\quad + \frac{\mu_y R_y^2}{\epsilon_z \mu_y k_0^2 - \beta_x^2} - \frac{\mu_z k_z^2}{\epsilon_y \mu_z k_0^2 - \beta_x^2}). \end{aligned} \tag{20}$$

Region II

$$\beta_x^2 - R_y^2 - k_{0z}^2 = k_0^2. \tag{21}$$

From Equations (19)–(21), it is seen that three equations with four unknowns  $\beta_x$ ,  $R_y$ ,  $k_z$ , and  $k_{0z}$  are obtained, which implies that there is no unique solution for  $\beta_x$ , unless  $R_y$  is determined. It is worth mentioning that for pure TM and TE surface waves,  $\beta_x$ ,  $k_z$ , and  $k_{0z}$  can be solved for given  $k_0$ , slab thickness  $t$ , and relative permittivity  $\bar{\epsilon}$  and permeability  $\bar{\mu}$  by substituting  $R_y = 0$  into Equations (19)–(21). The above analyses can also be applied to the grounded isotropic slab, in which case we can use the relative permittivity  $\epsilon_r = \epsilon_x = \epsilon_y = \epsilon_z$  and permeability  $\mu_r = \mu_x = \mu_y = \mu_z$ , instead of  $\bar{\epsilon}$  and  $\bar{\mu}$ .

### 2.2. Finite-Width Anisotropic Grounded Slab

Figure 2 shows the grounded anisotropic slab with a finite width  $2a$  and thickness  $t$ . By applying the boundary conditions at the interfaces  $y = \pm a$ , the propagation constant in the  $y$  direction  $R_y$  can then be determined. For analysis, the cross-section of the grounded slab is sub-divided into six regions, as shown in Figure 2b. Region I is the anisotropic slab, while the others are air regions. Since the fields in two corner Regions V and VI are very small, which are assumed to be negligible [22], we only take into account Regions I, II, III, and IV for analysis.

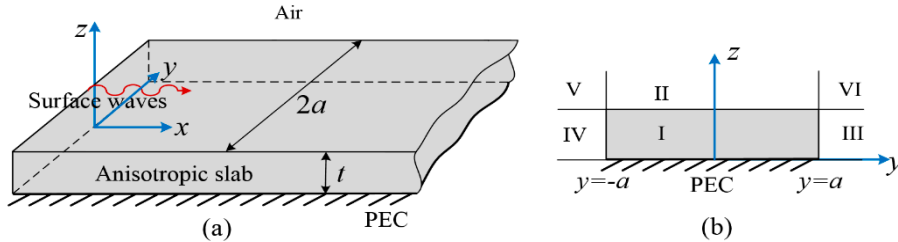


**Figure 2.** Surface waves on the interface of air region and grounded anisotropic slab with finite width: (a) Perspective view; and, (b) Cross-section view.

The E-field and H-field along the  $x$  direction for Regions I and II have the same expressions as Equations (2)–(5). However, due to the discontinuity at  $y = \pm a$ , reflected waves exist along the  $y$  direction. Therefore, the  $y$  components  $f_e(y)$  and  $f_h(y)$  of the E-Field and H-field are expressed as:

$$f_e(y) = e^{-R_y y} + r_1 e^{R_y y}, \quad (22)$$

$$f_h(y) = e^{-R_y y} + r_2 e^{R_y y}, \quad (23)$$

where  $r_1$  and  $r_2$  represent the magnitude ratios of  $e^{R_y y}$  and  $e^{-R_y y}$  for  $f_e(y)$  and  $f_h(y)$ , respectively. The fields in both Regions I and II in  $y$  and  $z$  directions can be obtained by substituting Equations (22) and (23) into Equations (7)–(14).

In Regions III and IV, the fields are decaying away from the interfaces  $y = \pm a$  along the  $y$  direction. Therefore, the  $y$  components of fields can be expressed as  $e^{-R_{0y} y}$  and  $e^{R_{0y} y}$ , respectively. Based on the continuity conditions of the tangent fields at the interface, the E-field and H-field along the  $x$  direction for Regions III and IV are given as follows:

Region III

$$E_x^{III} = A_{III} e^{-R_{0y} y} e^{-j\beta_x x} \sin(k_z z), \quad (24)$$

$$H_x^{III} = B_{III} e^{-R_{0y} y} e^{-j\beta_x x} \cos(k_z z), \quad (25)$$

Region IV

$$E_x^{IV} = A_{IV} e^{R_{0y} y} e^{-j\beta_x x} \sin(k_z z), \quad (26)$$

$$H_x^{IV} = B_{IV} e^{R_{0y} y} e^{-j\beta_x x} \cos(k_z z), \quad (27)$$

where  $A_{III}$ ,  $B_{III}$ ,  $A_{IV}$ , and  $B_{IV}$  are corresponding amplitude coefficients. The E-field and H-field in the  $y$  and  $z$  directions can then be found as:

Region III

$$E_y^{III} = \frac{e^{-j\beta_x x} e^{-R_{0y} y} \sin(k_z z)}{j(k_0^2 - \beta_x^2)} [-\beta_x R_{0y} A_{III} - \omega \mu_0 k_z B_{III}], \quad (28)$$

$$H_y^{III} = \frac{e^{-j\beta_x x} e^{-R_{0y} y} \cos(k_z z)}{j(k_0^2 - \beta_x^2)} [-\beta_x R_{0y} B_{III} - \omega \epsilon_0 k_z A_{III}], \quad (29)$$

$$E_z^{III} = \frac{e^{-j\beta_x x} e^{-R_{0y} y} \cos(k_z z)}{j(k_0^2 - \beta_x^2)} [\beta_x k_z A_{III} + \omega \mu_0 R_{0y} B_{III}], \quad (30)$$

$$H_z^{III} = \frac{e^{-j\beta_x x} e^{-R_{0y} y} \sin(k_z z)}{j(k_0^2 - \beta_x^2)} [-\beta_x k_z B_{III} - \omega \epsilon_0 R_{0y} A_{III}]. \quad (31)$$

Region IV

$$E_y^{IV} = \frac{e^{-j\beta_x x} e^{R_{0y} y} \sin(k_z z)}{j(k_0^2 - \beta_x^2)} [\beta_x R_{0y} A_{IV} - \omega \mu_0 k_z B_{IV}], \tag{32}$$

$$H_y^{IV} = \frac{e^{-j\beta_x x} e^{R_{0y} y} \cos(k_z z)}{j(k_0^2 - \beta_x^2)} [\beta_x R_{0y} B_{IV} - \omega \epsilon_0 k_z A_{IV}], \tag{33}$$

$$E_z^{IV} = \frac{e^{-j\beta_x x} e^{R_{0y} y} \cos(k_z z)}{j(k_0^2 - \beta_x^2)} [\beta_x k_z A_{IV} - \omega \mu_0 R_{0y} B_{IV}], \tag{34}$$

$$H_z^{IV} = \frac{e^{-j\beta_x x} e^{R_{0y} y} \sin(k_z z)}{j(k_0^2 - \beta_x^2)} [-\beta_x k_z B_{IV} + \omega \epsilon_0 R_{0y} A_{IV}]. \tag{35}$$

The boundary condition across the interface  $z = t$  provides the same result as Equation (19), while the field continuities at the interfaces  $y = \pm a$  give

$$\begin{aligned} & \beta_x^2 k_z^2 \left( \frac{1}{\epsilon_z \mu_y k_0^2 - \beta_x^2} - \frac{1}{k_0^2 - \beta_x^2} \right) \left( \frac{1}{\epsilon_y \mu_z k_0^2 - \beta_x^2} - \frac{1}{k_0^2 - \beta_x^2} \right) \\ &= k_0^2 \left( -\frac{\mu_y R_y}{\epsilon_z \mu_y k_0^2 - \beta_x^2} + \frac{R_{0y}}{k_0^2 - \beta_x^2} \frac{e^{-R_y a} - r_1 e^{R_y a}}{e^{-R_y a} + r_1 e^{R_y a}} \right) \left( -\frac{\epsilon_y R_y}{\epsilon_y \mu_z k_0^2 - \beta_x^2} \right. \\ & \quad \left. + \frac{R_{0y}}{k_0^2 - \beta_x^2} \frac{e^{-R_y a} + r_1 e^{R_y a}}{e^{-R_y a} - r_1 e^{R_y a}} \right), \end{aligned} \tag{36}$$

and

$$r_1 = -r_2 = \begin{cases} 1 \text{ quasi-TM mode} \\ -1 \text{ quasi-TE mode} \end{cases} \tag{37}$$

In addition, the dispersion relation of both Regions III and IV can be found as

$$\beta_x^2 - R_{0y}^2 + k_z^2 = k_0^2. \tag{38}$$

Therefore, from Equations (19)–(21) and (36)–(38), it is seen that six equations with six unknowns  $\beta_x$ ,  $R_y$ ,  $R_{0y}$ ,  $k_z$ ,  $k_{oz}$ , and  $r_1$  are derived, so that the propagation characteristics of the quasi-TM and quasi-TE surface waves can be determined.

### 3. Numerical Analysis

#### 3.1. Comparison of Different Methods

In this section, three different methods are employed to compare the propagation characteristics of surface waves on an anisotropic grounded dielectric slab. In the first method, it is assumed that the slab is infinitely large in both  $x$  and  $y$  directions, and there is no field variation along the  $y$  direction. This method has been utilized in most open literature, but it can only provide approximate results for real engineering applications, in which finite-width slabs are usually employed, and the field distributions along the  $y$  direction are non-uniform. The propagation characteristics are summarized in Equations (A1)–(A6) in Appendix A. The second method is based on Marcatili’s method [22]. This method considers the field variations along the  $y$  direction of the finite-width slab. However, the analysis assumes that  $H_z = 0$  and  $H_y = 0$  for quasi-TM and quasi-TE modes, respectively. Based on this approximate method, we derived the closed-form expressions for propagation characteristics of quasi-TM and quasi-TE modes for the considered structure, which can be obtained using Equations (B2)–(B6) and (B8)–(B12), respectively, as summarized in Appendix B. The third one is based on our derivations by using Equations (19)–(21) and (36)–(38). In our method, hybrid surface wave modes on grounded dielectric slab with finite width are analyzed, which addresses the main concern and provides a more accurate solution for practical applications.

As an example, we use an anisotropic PTFE substrate in [21] with  $\epsilon_x = 2.95$ ,  $\epsilon_y = 2.89$ ,  $\epsilon_z = 2.45$ , and  $\mu_x = \mu_y = \mu_z = 1$  to analyze the propagation constants of surface waves, and the results at  $f = 16$  GHz are shown in Figure 3a. In addition, the corresponding results of isotropic slab with  $\epsilon_x = \epsilon_y = \epsilon_z = 2.45$  and  $\mu_x = \mu_y = \mu_z = 1$  are also shown in Figure 3b for comparison. In our calculation, we are

looking for solutions that surface waves propagate along the  $x$  direction and decay in the  $z$  direction away from the interface, so that  $\beta_x$  and  $k_{0z}$  should be positive real numbers. For the first method, the slab width is assumed to be infinite with  $R_y = 0$ , while for the other two methods, the slab width is set as  $2a = 37.5$  mm, with  $R_y \neq 0$ . Figure 3a,b both indicate that the results of finite-width slab obtained by Macatili's method and our method are very close. However, it is interesting to note that for a fixed slab thickness, the propagation constant  $\beta_x$  obtained from the finite-width slab ( $R_y \neq 0$ ) is smaller than that from the infinite one ( $R_y = 0$ ). In other words, in order to excite the same order of surface waves with an equal  $\beta_k$ , the finite-width slab should be thicker than the infinite one. In addition, it is seen that as the thicknesses of finite- and infinite-width slabs decrease, the finite one can reach the condition  $\beta_k/k_0 = 1$  with a larger  $t$ . Under this condition, the surface waves will transform into leaky waves. Furthermore, comparing the case of anisotropic with isotropic slabs, it is seen that the anisotropic property of the slab has significant effects on both quasi-TM and quasi-TE modes, which will be discussed in detail in the next section.

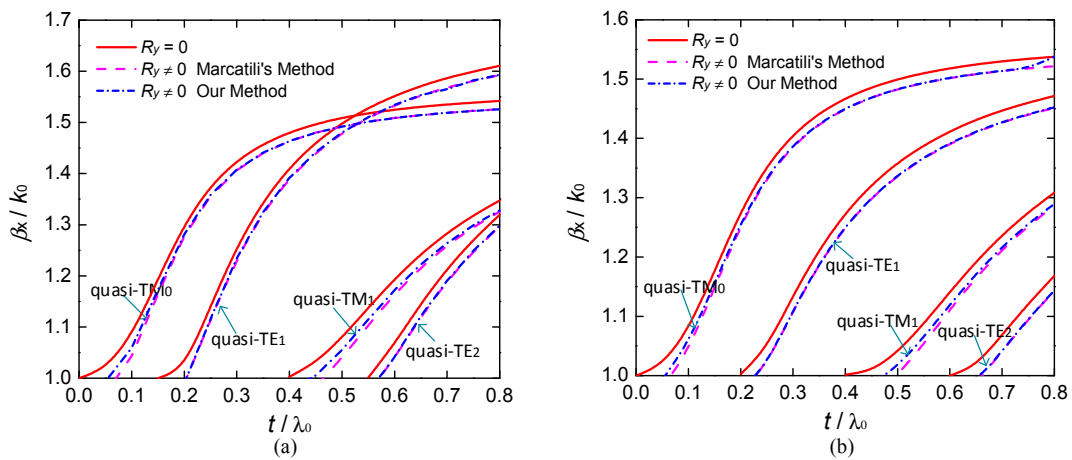


**Figure 3.** Comparison of  $\beta_x/k_0$  as a function of slab thickness  $t/\lambda_0$  for grounded dielectric slab, (a) anisotropic slab with  $\epsilon_x = 2.95$ ,  $\epsilon_y = 2.89$ ,  $\epsilon_z = 2.45$  and  $\mu_x = \mu_y = \mu_z = 1$ ; (b) isotropic slab with  $\epsilon_x = \epsilon_y = \epsilon_z = 2.45$ ,  $\mu_x = \mu_y = \mu_z = 1$ . ( $a = \infty$  for  $R_y = 0$ ,  $2a = 37.5$  mm for  $R_y \neq 0$ ).

As shown in Figure 4a, the values of  $\beta_x/k_0$  as a function of  $t/\lambda_0$  with different slab widths are compared. In this study, our method based on Equations (19)–(21) and (36)–(38) is employed for the case of finite-width slab, while for the case of  $a = \infty$ , the first method is utilized. It is seen that when the slab width increases, the values of  $\beta_x/k_0$  increase, and they are closer to the case of  $a = \infty$  with  $R_y = 0$ . This phenomenon also validates our derivations in a way. Furthermore, it is worth pointing out that the propagation constant in the  $y$  direction  $R_y$  is revealed to be a pure imaginary number in our calculation, which indicates that the surface waves propagate along the  $y$  direction in addition to the  $x$  direction, so that the propagating direction deviates from the  $x$  direction with some certain angle. The values of  $|\beta_x/R_y|$  as a function of  $t/\lambda_0$  with different slab widths are plotted in Figure 4b. The results indicate that  $|\beta_x/R_y|$  is very sensitive to the slab width. When the slab width increases, then the value of  $|\beta_x/R_y|$  increases significantly, meaning that the propagation direction is closer to the  $x$  direction.

### 3.2. Effects of Permittivity Tensor on Propagation Characteristics of Surface Waves

The effects of the relative permittivity tensor on propagation characteristics of surface waves are investigated. Based on Equations (19)–(21) and (36)–(38), the corresponding values of  $\beta_x/k_0$  and  $|\beta_x/R_y|$  as a function of slab thickness are calculated. As an instance, the calculated frequency is set as  $f = 16$  GHz, and the slab width is  $2a = 56.25$  mm.

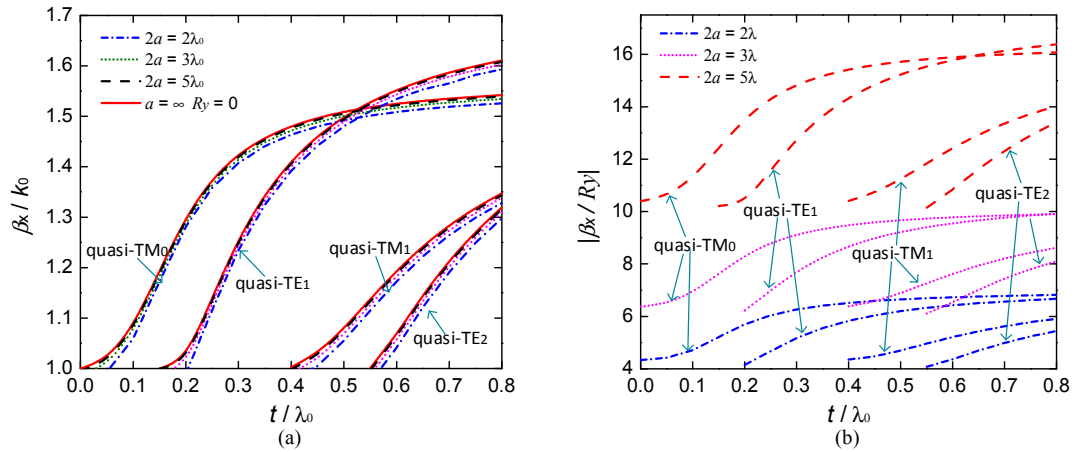


**Figure 4.** Effects of slab width on (a)  $\beta_x/k_0$  and (b)  $|\beta_x/R_y|$  as a function of slab thickness for grounded anisotropic slab. ( $\epsilon_x = 2.95$ ,  $\epsilon_y = 2.89$ ,  $\epsilon_z = 2.45$ ,  $\mu_x = \mu_y = \mu_z = 1$ ).

Figure 5a,d show the effects of  $\epsilon_x$  on  $\beta_x/k_0$  and  $|\beta_x/R_y|$  as a function of slab thickness. It is seen that when both  $\epsilon_y$  and  $\epsilon_z$  remain to be 2.45 and the value of  $\epsilon_x$  varies from 2.45 to 3.15,  $\beta_x/k_0$ , and  $|\beta_x/R_y|$  are almost stable for quasi-TE modes. However, the corresponding values of quasi-TM modes slightly change with the increase of  $\epsilon_x$ . Similarly, the effects of  $\epsilon_y$  and  $\epsilon_z$  on the propagation characteristics of surface waves are also investigated. Figure 5b,e illustrate that slightly increasing  $\epsilon_y$  results in a significant increase of  $\beta_x/k_0$  and  $|\beta_x/R_y|$  for quasi-TE modes, while the quasi-TM modes are nearly unaffected. In contrast, as shown in Figure 5c,f, the value of  $\epsilon_z$  can significantly affect the propagation characteristics of quasi-TM modes, but hardly contributes to the quasi-TE modes. Since most of the substrates exhibit a nonnegligible amount of anisotropy during the process of fabrication, these effects should be seriously taken into account for engineering applications. It should be mentioned that although the relative permittivity tensor can affect the propagation constants along both  $x$  and  $y$  directions, the slab width plays a major role in affecting the value of  $|\beta_x/R_y|$ , as displayed in Figure 4b. In addition, we also employ the other two methods discussed above to analyze these effects as well as to validate our derivation further. The phenomena are in good agreement by using different methods, and these discussions are omitted here for the sake of brevity.

### 3.3. Field Distributions of Surface Waves

The field distributions of surface waves propagating on a finite-width grounded dielectric slab are examined in this section. For instance, we use an anisotropic slab with  $\epsilon_x = 2.95$ ,  $\epsilon_y = 2.89$ ,  $\epsilon_z = 2.45$ , and  $\mu_x = \mu_y = \mu_z = 1$ . The slab width is = 400 mm. The height of the slab is  $t = 5$  mm ( $0.27\lambda_0$  at calculated frequency  $f = 16$  GHz). By substituting the values  $\beta_x$ ,  $R_y$ ,  $R_{0y}$ ,  $k_z$ ,  $k_{0z}$ , and  $r_1$  obtained from Equations (19)–(21) and (36)–(38) into Equations (7)–(14) and (24)–(35), the field distributions in all of the regions can be obtained. Based on Figure 3, it is known that when the slab thickness is  $0.27\lambda_0$ , quasi-TM<sub>0</sub>, and quasi-TE<sub>1</sub> surface wave modes are excited. Figure 6 shows the distributions of E- and H-field components of the quasi-TM<sub>0</sub> mode on the  $y$ - $z$  cut-plane at  $x = 0$  mm in Regions I and II. It should be mentioned that the magnitude of E-field component along the  $x$  direction  $|E_x|$  is normalized, and the magnitudes of other components are then obtained accordingly. Based on the field distributions of the quasi-TM<sub>0</sub> mode, the following phenomena are observed: (1) Most fields are trapped inside the slab and bound onto the interface at  $z = 5$  mm. When it is away from the interface, the field decay rapidly; (2) Due to the finite width of the slab, the fields non-uniformly distribute along the  $y$  direction; (3) Figure 6a shows that for the E-field components,  $|E_x|$  and  $|E_z|$  are much larger than  $|E_y|$ ; Figure 6b indicates that for the H-field components,  $|H_x|$  and  $|H_z|$  are very small compared to  $|H_y|$ ; (4) On the ground plane at  $t = 0$ , the tangential E-fields  $|E_x|$  and  $|E_y|$  are zero, while the normal component  $|E_z|$  is strong. On the other hand, for the H-fields,  $|H_x|$  and  $|H_y|$  are maximum, while  $|H_z|$  is zero when  $t = 0$ .

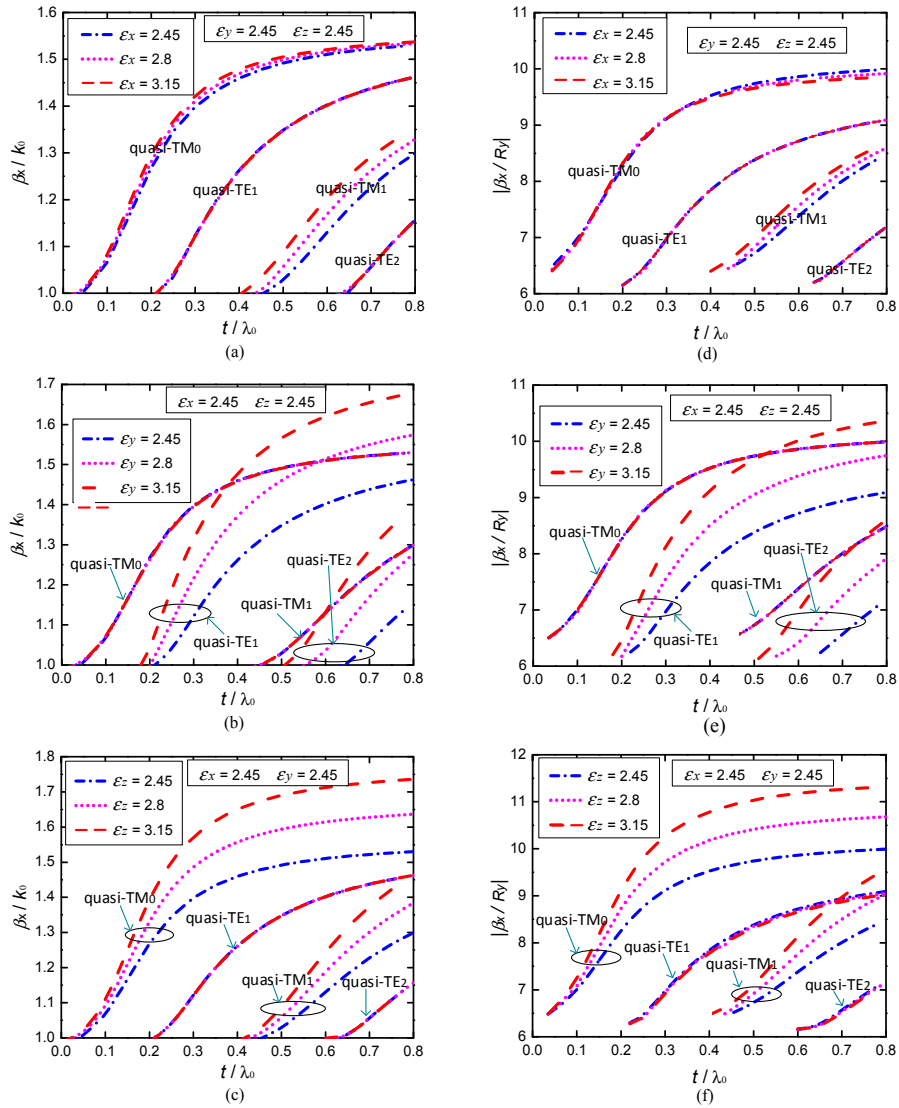


**Figure 5.** Effects of (a); (d)  $\epsilon_x$ ; (b); (e)  $\epsilon_y$ ; and (c,f)  $\epsilon_z$  on  $\beta_x/k_0$  and  $|\beta_x/R_y|$  as a function of slab thickness for grounded anisotropic slab with slab width of  $2a = 56.25$  mm.

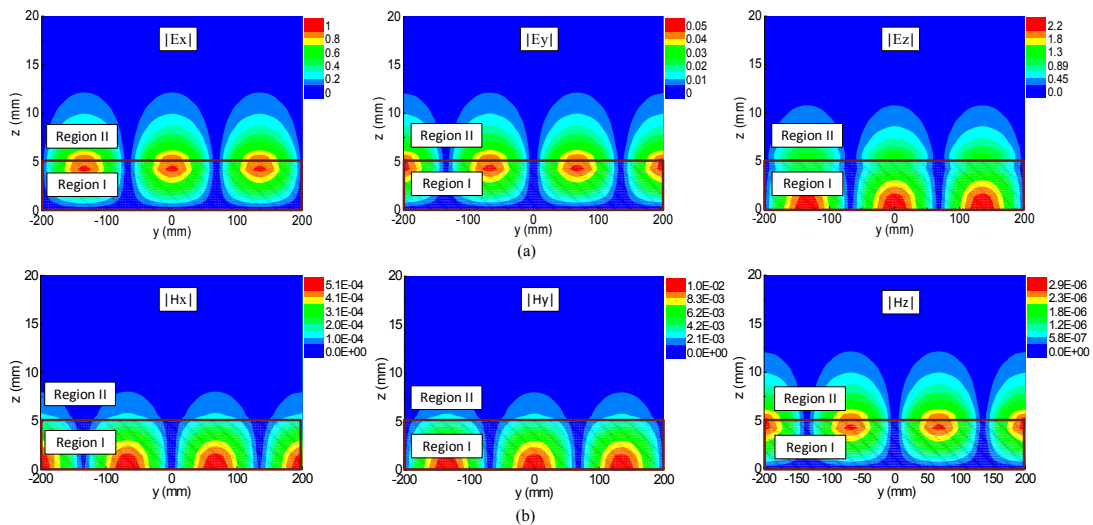


**Figure 6.** Distributions of (a) E-field and (b) H-field components of quasi-TM<sub>0</sub> mode when surface wave is propagation on the finite-width grounded anisotropic slab. ( $y$ - $z$  cut-plane at  $x = 0$  mm,  $t = 5$  mm,  $2a = 400$  mm,  $\epsilon_x = 2.95$ ,  $\epsilon_y = 2.89$ ,  $\epsilon_z = 2.45$ ,  $\mu_x = \mu_y = \mu_z = 1$ ,  $f = 16$  GHz).

In addition, the field distributions of quasi-TE<sub>1</sub> mode on the  $y$ - $z$  cut-plane at  $x = 0$  mm are plotted in Figure 7. Several similar phenomena are observed when compared to Figure 6. However, contrary to the quasi-TM<sub>0</sub> mode, it is seen from Figure 7a that the E-field components of quasi-TE<sub>1</sub> mode  $|E_x|$  and  $|E_z|$  are small as compared to  $|E_y|$ . While for the H-field distributions in Figure 7b,  $|H_x|$  and  $|H_z|$  are much larger than  $|H_y|$ . These reasonable observations further prove the reliability of our proposed method. It is also expected that the proposed method is very promising for analyzing other higher-order surface wave modes for a thicker slab.

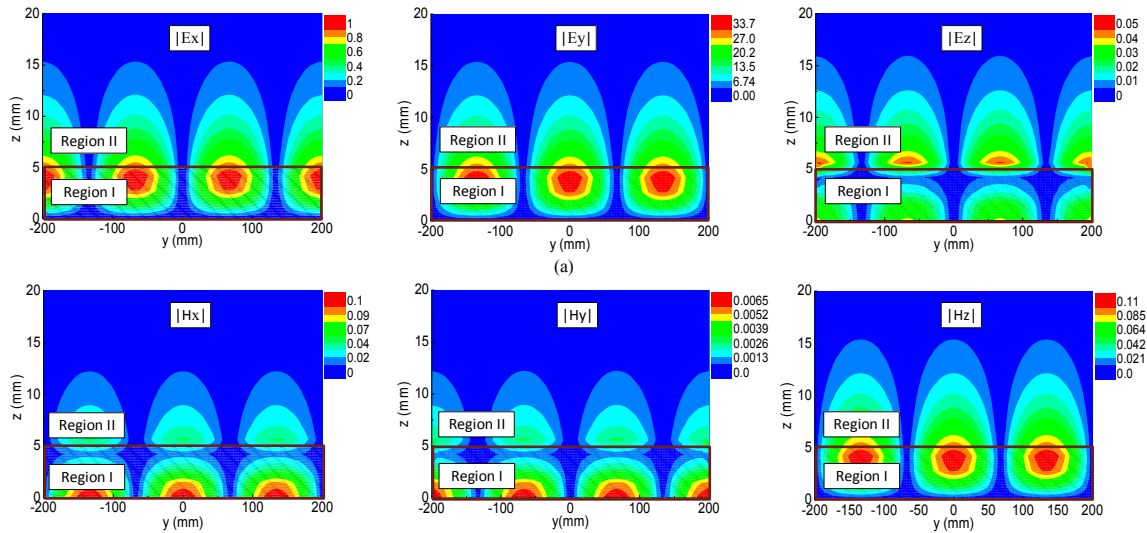


**Figure 7.** Distributions of (a) E-field and (b) H-field components of quasi-TE<sub>1</sub> mode when surface wave is propagation on the finite-width grounded anisotropic slab. ( $y$ - $z$  cut-plane at  $x = 0$  mm,  $t = 5$  mm,  $2a = 400$  mm,  $\epsilon_x = 2.95$ ,  $\epsilon_y = 2.89$ ,  $\epsilon_z = 2.45$ ,  $\mu_x = \mu_y = \mu_z = 1$ ,  $f = 16$  GHz).

#### 4. Conclusions

In conclusion, we have proposed a method to analyze the surface waves propagating on grounded anisotropic slab. Different from most open literatures, which generally assume that the fields of surface waves uniformly distribute along the transverse direction of the infinitely large grounded slab, we have thoroughly considered the field variations in the direction transverse to the wave propagation direction, and the corresponding propagation characteristics of surface waves have been derived on the basis of boundary conditions and Maxwell’s equations. Three different methods have been employed to analyze the surface waves on grounded anisotropic slab as well as to validate our derivations. The effects of the relative permittivity tensor on the propagation characteristics of surface waves have been also numerically studied. In addition, the field distributions of surface waves have been examined with the aid of the proposed method. More importantly, our method takes into account the finite-width grounded slab with the fields non-uniformly distributing along the transverse direction of the slab, which is more suitable for practical engineering.

**Author Contributions:** Zhuozhu Chen derived the formula, analyzed the data, and wrote the paper. Zhongxiang Shen conceived the idea, provided the suggestions, and revised the manuscript.

**Conflicts of Interest:** The authors declare no conflict of interest.

#### Appendix A. Derivation of Surface Waves Uniformly Distributed on Grounded Anisotropic Slab

For the grounded slab with infinite width as shown in Figure 1, pure TM or TE mode can be supported if the field distribution of surface wave along the transversal direction of the slab is assumed to be uniform ( $R_y = 0$ ), as analyzed in Section 2.1.

For TM surface wave, substituting  $B_I = B_{II} = 0$  into Equations (7)–(14) and applying continuity conditions of all the tangential fields across the interface lead to:

$$k_z \tan(k_z t) = \epsilon_x k_{oz} . \tag{A1}$$

By solving Maxwell’s equation, the dispersion relations in Regions I and II can be derived as:

Region I

$$\beta_x^2 + \frac{\epsilon_z}{\epsilon_x} k_z^2 = \epsilon_z \mu_y k_0^2. \tag{A2}$$

Region II

$$\beta_x^2 - k_{0z}^2 = k_0^2. \tag{A3}$$

For TE surface wave,  $A_I = A_{II} = 0$ . Similarly, the boundary conditions and the dispersion relations in the anisotropic medium and air regions lead to:

$$k_z \cot(k_z t) = -\mu_x k_{oz}, \tag{A4}$$

$$\beta_x^2 + \frac{\mu_z}{\mu_x} k_z^2 = \epsilon_y \mu_z k_0^2, \tag{A5}$$

$$\beta_x^2 - k_{0z}^2 = k_0^2. \tag{A6}$$

### Appendix B. Derivation of Surface Wave Modes Based on Marcatili’s Method

In [22], Marcatili introduced an approximate method to describe how the guided waves propagate through rectangular dielectric optical waveguides. Based on his method, the surface waves are divided into  $E^z$  and  $E^y$  modes. For  $E^z$  mode, the field component  $E_z$  is strong, while  $H_z$  is assumed to be zero, which represents the quasi-TM mode in our discussion. Similarly, the  $E^y$  mode represents quasi-TE mode in our discussion, in which case the field  $E_y$  is strong and  $H_y$  is assumed to be zero. In addition, the fields in Regions V and VI as shown in Figure 2b are assumed to be negligible. Based on these assumptions, the quasi-TM and quasi-TE modes can be analyzed separately.

For quasi-TM mode,  $H_z$  and  $H_y$  of Regions I, II, III, and IV can be expressed as:

$$H_z^I = H_z^{II} = H_z^{III} = H_z^{IV} = 0, \tag{B1}$$

$$H_y^I = A_I(e^{-R_y y} + r_1 e^{R_y y})e^{-j\beta_x x} \cos(k_z z), \tag{B2}$$

$$H_y^{II} = A_{II}(e^{-R_y y} + r_1 e^{R_y y})e^{-j\beta_x x} e^{-k_{0z} z}, \tag{B3}$$

$$H_y^{III} = A_{III} e^{-R_{0y} y} e^{-j\beta_x x} \cos(k_z z), \tag{B4}$$

$$H_y^{IV} = A_{IV} e^{R_{0y} y} e^{-j\beta_x x} \cos(k_z z). \tag{B5}$$

Based on the fields  $H_z$  and  $H_y$ , all field distributions and dispersion relations in four regions can then be derived by solving Maxwell’s equations.

The continuity conditions of  $E_x$  and  $H_y$  at  $z = t$  give

$$k_z \tan(k_z t) = \epsilon_x k_{oz}. \tag{B6}$$

In addition,  $E_z$  and  $H_x$  are continuous at  $y = \pm a$ , which leads to:

$$R_{0y} \mu_x (\epsilon_x \mu_y k_0^2 - k_z^2) \frac{e^{-R_y a} + e^{R_y a}}{e^{-R_y a} - e^{R_y a}} = \epsilon_x \mu_y R_y (k_0^2 - k_z^2). \tag{B7}$$

The dispersion relations in four regions are derived as:

$$\beta_x^2 - \frac{\mu_y}{\mu_x} R_y^2 + \frac{\epsilon_z}{\epsilon_x} k_z^2 = \epsilon_z \mu_y k_0^2, \tag{B8}$$

$$\beta_x^2 - R_y^2 - k_{0z}^2 = k_0^2, \tag{B9}$$

$$\beta_x^2 - R_{0y}^2 + k_z^2 = k_0^2. \tag{B10}$$

It is seen that  $\beta_x$ ,  $R_y$ ,  $R_{0y}$ ,  $k_z$ , and  $k_{oz}$  can be solved for given  $k_0$ ,  $t$ ,  $\bar{\epsilon}$ ,  $\bar{\mu}$  based on Equations (B6)–(B10).

For quasi-TE mode,  $H_y$  and  $H_z$  in Regions I, II, III, and IV can be expressed as:

$$H_y^I = H_y^{II} = H_y^{III} = H_y^{IV} = 0, \quad (B11)$$

$$H_z^I = B_I(e^{-R_y y} + r_2 e^{R_y y})e^{-j\beta_x x} \sin(k_z z), \quad (B12)$$

$$H_z^{II} = B_{II}(e^{-R_y y} + r_2 e^{R_y y})e^{-j\beta_x x} e^{-k_{0z} z}, \quad (B13)$$

$$H_z^{III} = B_{III} e^{-R_{0y} y} e^{-j\beta_x x} \sin(k_z z), \quad (B14)$$

$$H_z^{IV} = B_{IV} e^{R_{0y} y} e^{-j\beta_x x} \sin(k_z z). \quad (B15)$$

Similarly, based on Maxwell's equations and boundary conditions, five equations with five unknowns  $\beta_x$ ,  $R_y$ ,  $R_{0y}$ ,  $k_z$ , and  $k_{0z}$  can be derived, and they are summarized below:

$$-k_z \cot(k_z t) = \mu_x k_{0z}, \quad (B16)$$

$$R_y(k_0^2 + R_0^2) \frac{e^{-R_y a} - e^{R_y a}}{e^{-R_y a} + e^{R_y a}} = R_{0y} \epsilon_y (\epsilon_x \mu_z k_0^2 + R_y^2), \quad (B17)$$

$$\beta_x^2 - \frac{\epsilon_y}{\epsilon_x} R_y^2 + \frac{\mu_z}{\mu_x} k_z^2 = \epsilon_y \mu_z k_0^2, \quad (B18)$$

$$\beta_x^2 - R_y^2 - k_{0z}^2 = k_0^2, \quad (B19)$$

$$\beta_x^2 - R_{0y}^2 + k_z^2 = k_0^2. \quad (B20)$$

## References

1. Dyakonov, M.I. New type of electromagnetic wave propagating at an interface. *Sov. Phys. JETP* **1988**, *67*, 714–716.
2. Artigas, D.; Torner, L. Dyakonov surface waves in photonic metamaterials. *Phys. Rev. Lett.* **2005**, *94*, 013901.
3. Chen, S.; Shen, Z.; Wu, W. Analysis of dyakonov surface waves existing at the interface of an isotropic medium and a conductor-backed uniaxial slab. *J. Opt. Soc. Am. A* **2014**, *31*, 1923–1930.
4. Pozar, D.M. *Microwave Engineering*, 3rd ed.; Wiley: New York, NY, USA, 2005.
5. Liu, S.H.; Liang, C.H.; Ding, W.; Chen, L.; Pan, W.T.; Electromagnetic wave propagation through a slab waveguide of uniaxially anisotropic dispersive metamaterial. *Prog. Electromagn. Res.* **2007**, *76*, 467–475.
6. Nevels, R.D.; Michalski, K.A. On the behavior of surface plasmons at a metallo-dielectric interface. *J. Lightwave Technol.* **2014**, *32*, 3299–3305.
7. Smith, D.R.; Schurig, D. Electromagnetic wave propagation in media with indefinite permittivity and permeability tensors. *Phys. Rev. Lett.* **2003**, *90*, 077405.
8. Yan, W.; Shen, L.; Ran, L.; Kong, J.A. Surface modes at the interfaces between isotropic media and indefinite media. *J. Opt. Soc. Am. A* **2007**, *24*, 530–535.
9. Volakis, J.L. *Antenna Engineering Handbook*, 4th ed.; McGraw-Hill: New York, NY, USA, 2007.
10. Knoesen, A.; Gaylord, T.K.; Moharam, M.G. Hybrid guided modes in uniaxial dielectric planar waveguides. *J. Lightwave Technol.* **1988**, *6*, 1083–1104.
11. Maldonado, T.A.; Gaylord, T.K. Hybrid guided modes in biaxial planar waveguides. *J. Lightwave Technol.* **1996**, *14*, 486–499.
12. Seshadri, S.R.; Pickard, W.F. Surface waves on an anisotropic plasma sheath. *IEEE Trans. Microw. Theory Tech.* **1964**, *12*, 529–541.
13. Engheta, N.; Pelet, P. Surface waves in chiral layers. *Opt. Lett.* **1991**, *16*, 723–725.
14. Rockstuhl, C.; Lederer, F. Intrinsic surface and bulk defect modes in quasi-periodic photonic crystals. *J. Lightwave Technol.* **2007**, *25*, 2299–2305.
15. Attwood, S.S. Surface-wave propagation over a coated plane conductor. *J. Appl. Phys.* **1951**, *22*, 504–509.
16. Liu, S.; Chen, L.; Liang, C. Guided modes in a grounded slab waveguide of uniaxially anisotropic left-handed material. *Microw. Opt. Technol. Lett.* **2007**, *49*, 1644–1648.
17. Baccarelli, P.; Burghignoli, P.; Frezza, F.; Galli, A.; Lampariello, P.; Lovat, G.; Paulotto, S. Fundamental modal properties of surface waves on metamaterial grounded slabs. *IEEE Trans. Microw. Theory Tech.* **2005**, *53*, 1431–1442.

18. Chen, Z.; Shen, Z. Wideband flush-mounted surface wave antenna of very low profile. *IEEE Trans. Antennas Propag.* **2015**, *63*, 2430–2438.
19. Jiang, Z.H.; Wu, Q.; Brocker, D.E.; Sieber, P.E.; Werner, D.H. A low-profile high-gain substrate-integrated waveguide slot antenna enabled by an ultrathin anisotropic zero-index metamaterial coating. *IEEE Trans. Antennas Propag.* **2014**, *62*, 1173–1184.
20. Jiang, Z.H.; Wu, Q.; Werner, D.H. Demonstration of enhanced broadband unidirectional electromagnetic radiation enabled by a subwavelength profile leaky anisotropic zero-index metamaterial coating. *Phys. Rev. B* **2012**, *86*, 125131.
21. Olyphant, M. Measuring anisotropy in microwave substrates. In Proceedings of the 1979 IEEE MTT-S International Microwave Symposium Digest, Orlando, FL, USA, 30 April–2 May 1979.
22. Marcatali, E.A.J. Dielectric rectangular waveguide and directional coupler for integrated optics. *Bell Syst. Tech. J.* **1969**, *48*, 2071–2102.



© 2018 by the authors. Licensee MDPI, Basel, Switzerland. This article is an open access article distributed under the terms and conditions of the Creative Commons Attribution (CC BY) license (<http://creativecommons.org/licenses/by/4.0/>).